Buckling of woven fibre and graphene platelet reinforced nanocomposite laminates

K Sewnath[1], G Drosopoulos[2,3], S Adali[1]

[1]Discipline of Mechanical Engineering, University of KwaZulu-Natal, Durban 4041, South Africa

[2]Discipline of Civil Engineering, University of Central Lancashire, Preston PR1 2HE, United Kingdom

[3]Discipline of Civil Engineering, University of KwaZulu-Natal, Durban 4041, South Africa

Abstract

Buckling of a hybrid laminate combining woven glass fibres with graphene platelets in a polymer matrix is the subject of the present study. Multiscale composites provide improved stiffness and light weigh laminates and as such they have become the materials of choice in several applications. The elastic properties of 3-phase materials are determined by using micromechanical relations. In the present study, the elastic constants of the woven fabric are computed first and the second step involves extending the micromechanical computations to determine the properties of the 3-phase woven fabric-graphene reinforced matrix. The objective is to improve the buckling capacity of the woven fabric laminates with high stiffness and light weight graphene reinforcement. Analytical results are given for the buckling load for a simply supported and orthotropic laminate, taking into account the complex pattern of woven fabrics consisting of weft and warp fibres. Numerical results illustrate the effect of the design parameters such as the layer thicknesses, fibre and graphene contents and aspect ratio on the buckling load. In particular, the effectiveness of the graphene reinforcement on improving buckling load is illustrated by means of contour plots.

Keywords: Buckling; Woven Fibres; Graphene Nanoplatelets; 3-Phase Laminate; Analytical Solution; Micromechanics Equations

1. Introduction

The use of woven fabrics as reinforcement material has a number of advantages as compared to fibre composites. These include thicker fibre forms, ease of handling and improved fracture toughness as noted in [1, 2, 3]. Textile composites such as woven fabric composites primarily find applications

in aerospace, marine, transportation, construction and power generation industries as noted in a number of publications and review articles [4, 5, 6, 7, 8].

A recent development is to improve the properties of composites by incorporating nano scale reinforcements in the matrix such as carbon nanotubes and graphene platelets. The inclusion of nanotubes and graphene as a reinforcing material has been the subject of a number of review articles [9, 10, 11]. It was noted that nano reinforcements resulted in the improvement of the overall properties of the composites resulting in higher stiffness and strength as well as lower weight due to low density of nano materials. For example, it was noted that graphene reinforced composites exhibit improved mechanical properties at weight fractions as low as 0.1% [12]. There have been other studies on the effect of small amounts of graphene on the properties of the composites. Studies [13, 14, 15, 16] observed that nanocomposites based on reinforcement using graphene displayed vastly improved mechanical properties. Several other studies on graphene nanocomposites provided extensive information not only on their properties as in [17, 18, 19], but also on issues involving their fabrication and applications [20, 21].

By using nanoscale reinforcements incorporated into glass or carbon fibre composites, the strength and stiffness of the composite can be improved further. One of the nanoscale reinforcements is carbon nanotubes due to their high Young's modulus, tensile strength and thermal conductivity [22]. More recently, graphene nanoplatelets have been used in multiscale composites due to their excellent physical and electronic properties [23]. Presently, they are one of the strongest materials available with a Young's modulus in the region of 1 TPa [24, 25].

Recent studies involved the use of graphene platelets in combination with fibre reinforcements leading to multiscale composites [26, 27, 28]. The elastic properties of composites can be determined by micromechanical relations which has been the subject of a number of studies [29, 30]. Micromechanics has been implemented to determine the elastic moduli of graphene sheet reinforced nanocomposites in [31]. In the case of woven fabric composites, the elastic constants were determined by means of micromechanical modelling in [32, 33, 34]. Graphene platelets are 2D structures and as such they have higher reinforcing capabilities compared to not only fibres but also carbon nanotubes. This is due to higher surface areas resulting better load transfer between the matrix and the reinforcement. Moreover, less agglomeration was observed in graphene platelet reinforced polymers as compared to one-dimensional carbon nanotubes. Graphene platelets as reinforcement were used in a number of studies involving the buckling of composite structures. Recent work involving the buckling of composite structures reinforced with graphene platelets include beams [35, 36], plates [37-46] and shells [47, 48].

Present study involves a hybrid composite laminate which combines woven glass fibres with graphene nanoplatelets as reinforcements. This combination improves the buckling capacity of the

laminate substantially by taking advantage of high stiffness and light weight of graphene reinforcement. The article provides an analytical solution for the buckling load taking into account the complex pattern of the proposed material. As shown in the subsequent sections, this complexity is due to the presence of weft and warp fibres, constituting the fibre reinforcement, as well as to the presence of graphene reinforcement. The article proposes a framework of micromechanics equations that can be used to determine the effective material properties of the 3-phase material. An effort is made to address the influence of several material parameters on the mechanical response of the multi-scale structure. To the authors' best knowledge, no similar articles can be found in the literature. In addition, most of the existing studies on woven fabrics mainly focus on either experimental investigation or numerical analysis using the finite element method. On the contrary, the present article provides an alternative, analytical solution to the buckling problem. The benefits of this approach are the low computational cost and the relatively simple numerical implementation in a programming code (e.g. MATLAB). These aspects highlight further the novelty of the article.

Mechanical properties of woven fabric reinforced laminate are determined by means of micromechanical relations. Next, the properties of hybrid woven fabric-graphene platelet reinforced polymer are determined using a different set of micromechanical relations. The buckling results are given for simply supported rectangular laminates subject to biaxial or uniaxial compression. The effect of problem parameters on the buckling load are investigated by means of 2D and contour graphs. The problem parameters include the volume and weight contents of the woven fabric and the graphene platelets, aspect ratio and the layer thicknesses. It is observed that a small amount of graphene platelets improves the buckling capacity of the laminates substantially.

2. Woven fabric micromechanical relations

Micromechanical relations to determine the elastic constants of a woven fabric material with plies having fibres at 0° and 90° orientations were first given in [49]. But the concept which is adopted in this article for the calculation of the effective material properties of woven fabric laminates and all relevant equations can be found in the book presented in [50]. The key idea for studying woven fabrics in this book is to adopt the "laminate analogy", according to which each cloth-reinforced layer consists of two unidirectional "sub-layers": one warp unidirectional sub-layer oriented at 0^o and one weft unidirectional sub-layer oriented at 90^o. This is schematically shown later in the article (in Figure 1). In this section micromechanical relations taken from [50] are provided, to compute the effective material properties between the two sub-layers (warp-weft). In section 5 it will be shown how these micromechanical relations can be used to determine the effective material properties of the 3-phase graphene/woven fabric laminate of this study.

The fibres aligned in the longitudinal direction are called the warp fibres and the fibres aligned in the transverse direction are called the weft fibres. The thicknesses of the warp layer and the weft layer are denoted by e_{wp} and e_{wf}, respectively. The warp layer is described by its longitudinal elastic modulus $E_{11_{wp}}$, transverse elastic modulus $E_{22_{wp}}$, Poisson's ratio $\nu_{12_{wp}}$ and shear modulus $G_{12_{wp}}$. Corresponding material constants for the weft layer are denoted as $E_{11_{wf}}$, $E_{22_{wf}}$, $\nu_{12_{wf}}$, and $G_{12_{wf}}$. A balancing coefficient k denotes the ratio of threads in the warp direction to threads in the weft direction by their volumes, v_{wp} and v_{wf} and is defined as

$$k = \frac{v_{wp}}{v_{wp} + v_{wf}} \tag{1}$$

For a woven fabric with $k = 0.5$, the fabric contains equal volumes of fibres in the warp and weft directions and, as such, is balanced with respect to the warp and weft fibres. The thicknesses of the warp and weft layers, denoted as e_{wp} and e_{wf}, are functions of the woven fibre balancing coefficient k, given in Eq. (1), and the total lamina thickness e, that is,

$$e_{wp} = ke\,; \quad e_{wf} = (1-k)e \tag{2}$$

The volume fraction V_{wp} of the warp layer is the ratio of the volume of the warp fibres to the total volume of the entire laminate (containing both warp and weft fibres). The volume fraction V_{wf} of the weft layer is the ratio of the weft fibres to the volume of the entire laminate. Thus $V_{ftot} = V_{wp} + V_{wf}$ is the total volume fraction of all fibres (both the warp and weft fibres) for the laminate. Two parameters, namely, α_{wp} and α_{wf} are defined as [50]:

$$\alpha_{wp} = \frac{1}{1 - \left(\frac{E_{22_{wp}}}{E_{11_{wp}}}\right)\nu_{12_{wp}}^2} \quad ; \qquad \alpha_{wf} = \frac{1}{1 - \left(\frac{E_{22_{wf}}}{E_{11_{wf}}}\right)\nu_{12_{wf}}^2} \tag{3}$$

The expressions for the in-plane moduli of a lamina of the woven fabric, E_{11}, E_{22}, ν_{12} and G_{12}, can be expressed as functions of α_{wp}, α_{wf}, $E_{11_{wp}}$, $E_{22_{wp}}$, $E_{11_{wf}}$, $E_{22_{wf}}$, $\nu_{12_{wp}}$, $\nu_{12_{wf}}$, $G_{12_{wp}}$, $G_{12_{wf}}$, and k as follows:

$$E_{11} = (1-\alpha)\left(k\alpha_{wp}E_{11_{wp}} + (1-k)\alpha_{wf}E_{22_{wf}}\right) \tag{4}$$

$$E_{22} = (1-\alpha)\left(k\alpha_{wp}E_{22_{wp}} + (1-k)\alpha_{wf}E_{11_{wf}}\right) \tag{5}$$

$$\nu_{12} = \frac{k\alpha_{wp}\nu_{12_{wp}}E_{22_{wp}} + (1-k)\alpha_{wf}\nu_{12_{wf}}E_{22_{wf}}}{k\alpha_{wp}E_{22_{wp}} + (1-k)\alpha_{wf}E_{11_{wf}}} \tag{6}$$

$$G_{12} = kG_{12_{wp}} + (1-k)G_{12_{wf}} \tag{7}$$

The parameter α is calculated from the equation

$$\alpha = \frac{\left[k\alpha_{wp}v_{12_{wp}}E_{22_{wp}} + (1-k)\alpha_{wf}v_{12_{wf}}E_{22_{wf}}\right]^2}{\left[k\alpha_{wp}E_{11_{wp}} + (1-k)\alpha_{wf}E_{22_{wf}}\right]\left[k\alpha_{wp}E_{22_{wp}} + (1-k)\alpha_{wf}E_{11_{wf}}\right]} \tag{8}$$

3. Simply-supported laminate subject to biaxial loading

The reduced stiffness matrix in the principal directions of a laminate for the k^{th} layer is given by

$$Q_k = \begin{bmatrix} Q_{11} & Q_{12} & 0 \\ Q_{12} & Q_{22} & 0 \\ 0 & 0 & Q_{66} \end{bmatrix}_k \tag{9}$$

The Q_{ij} terms in Eq. (9) are expressed as functions of longitudinal elastic modulus E_{11}, transverse elastic modulus E_{22}, Poisson's ratio v_{12}, and longitudinal shear modulus G_{12} as

$$Q_{11} = \frac{E_{11}}{1 - \left(\frac{E_{22}}{E_{11}}\right)v_{12}^2} \quad ; \quad Q_{22} = \frac{E_{22}}{1 - \left(\frac{E_{22}}{E_{11}}\right)v_{12}^2} \tag{10}$$

$$Q_{12} = v_{12}Q_{22} \quad ; \quad Q_{66} = G_{12} \tag{11}$$

The equation governing the buckling of an orthotropic and symmetrical laminate based on the classical laminate theory is given by

$$D_{11}\frac{\partial^4 w_o}{\partial x^4} + 2(D_{12} + 2D_{66})\frac{\partial^4 w_o}{\partial x^2 \partial y^2} + D_{22}\frac{\partial^4 w_o}{\partial y^4} = N_x\frac{\partial^2 w_o}{\partial x^2} + N_y\frac{\partial^2 w_o}{\partial y^2} \tag{12}$$

where N_x and N_y are the biaxial buckling loads in the x and y directions, respectively. For a laminate with k layers, and defining h_n as the distance from the midpoint of the laminate to the top of the n_{th} layer, D_{ij} is given by

$$D_{ij} = \frac{1}{3}\sum_{n=1}^{k}(h_n^3 - h_{n-1}^3)\left(Q_{ij}\right)_n \tag{13}$$

For a plate of dimensions $a \times b$, the solution for w_o satisfying the simply supported boundary conditions is given by

$$w_o(x,y) = A_{mn}\sin\left(\frac{m\pi x}{a}\right)\sin\left(\frac{n\pi y}{b}\right) \tag{14}$$

where m and n are the number of half-waves in the x and y directions. The aspect ratio R of the rectangular plate is $R = a/b$, and the buckling ratio α_b is defined as $\alpha_b = N_y/N_x$. The buckling load is determined by minimizing N_{cr} with respect to m and n and is given by

$$N_{cr} = \min \frac{\pi^2(D_{11}m^4 + 2(D_{12} + 2D_{66})\, m^2n^2R^2 + D_{22}n^4R^4)}{a^2(m^2 + \alpha_b n^2R^2)} \tag{15}$$

4. Woven fabric reinforced laminate

The symmetrically laminated orthotropic plate under consideration consists of four layers and is subject to biaxial or uniaxial buckling loads. Surface (top and bottom) layers are of the same thickness which is denoted by e_o where the subscript "o" indicates the outer layers as shown in Figure 1. The two middle layers of equal thickness are denoted as e_m. Thus, the total thickness of the laminate is $H = 2(e_o + e_m)$. The thicknesses of the outer and middle layers could be different and as such the laminate can have non-uniform layer thicknesses, that is, $e_o \neq e_m$ (Figure 1). The fibre orientations of the outer (surface) and middle layers are denoted as θ_o and θ_m, respectively. The matrix of the laminate is reinforced by woven fabric and graphene platelets leading to a 3-phase nanocomposite. Apart from the thicknesses of the outer and middle layers being non-uniform, the reinforcements are also distributed non-uniformly across the thickness, i.e., the volume contents of the woven fabric and the graphene platelets in the outer and middle layers could be different. The layers of the laminate are labelled as $n = 1,2,3,4$ starting from the bottom layer. The warp and weft fibres of the layers are indicated as lines and dots as shown in Figure 1. It is noted that middle layers have the same fibre and graphene contents and fibre orientations and the same applies to the outer layers.

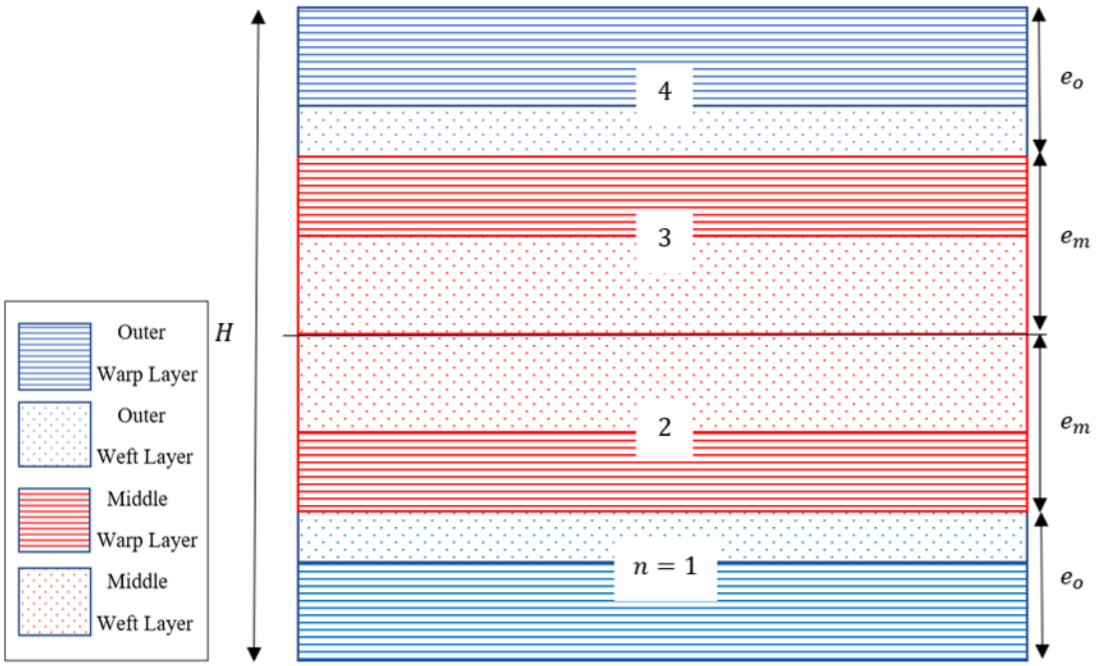

Figure 1. 4-layer, symmetric, woven fibre and graphene platelet reinforced laminated plate

The thickness ratio τ is defined as the ratio of the total thickness of the outer layers to the total laminate thickness H, that is,

$$\tau = \frac{2e_o}{H} \tag{16}$$

where $0 \leq \tau \leq 1$ with $\tau = 0$ corresponding to a laminate with the middle layers only and $\tau = 1$ to a laminate with outer layers only.

4.1. Reduced stiffness terms

The reduced stiffness terms, which were provided by equations (10), (11) in Section 3, are given here in the context of the adopted 4-layer woven fabric laminate. Let Q_{ijn} denote the reduced stiffness terms in the n^{th} layer ($n = 1,2,3,4$) and let $p = o$ denote the outer layers ($n = 1,4$) and $p = m$ denote the middle layers ($n = 2,3$). The reduced stiffness terms are given by [50]:

$$Q_{11p} = \alpha_p E_{11p}; \qquad Q_{12p} = \alpha_p \nu_{12p} E_{22p} \tag{17}$$

$$Q_{22p} = \alpha_p E_{22p}; \qquad Q_{66p} = G_{12p} \tag{18}$$

where

$$\alpha_p = \frac{1}{1 - \frac{E_{22p}}{E_{11p}} \nu_{12p}^2} \tag{19}$$

In Figure 2, the expressions for the thickness of each sublayer (warp and weft layers of each lamina) are shown on the left. The subscripts wp and wf denote the warp and weft layers, respectively. The woven fibre balancing coefficient, k_o or k_m, indicates the thickness of each sublayer. Since the laminate is symmetrical about the midpoint, it has two outer layers whose widths are e_o and balancing coefficient k_o, and two middle layers with e_m and k_m. The distance from the midpoint to the top of the middle layer is denoted as $c = e_m$ as shown in Figure 2.

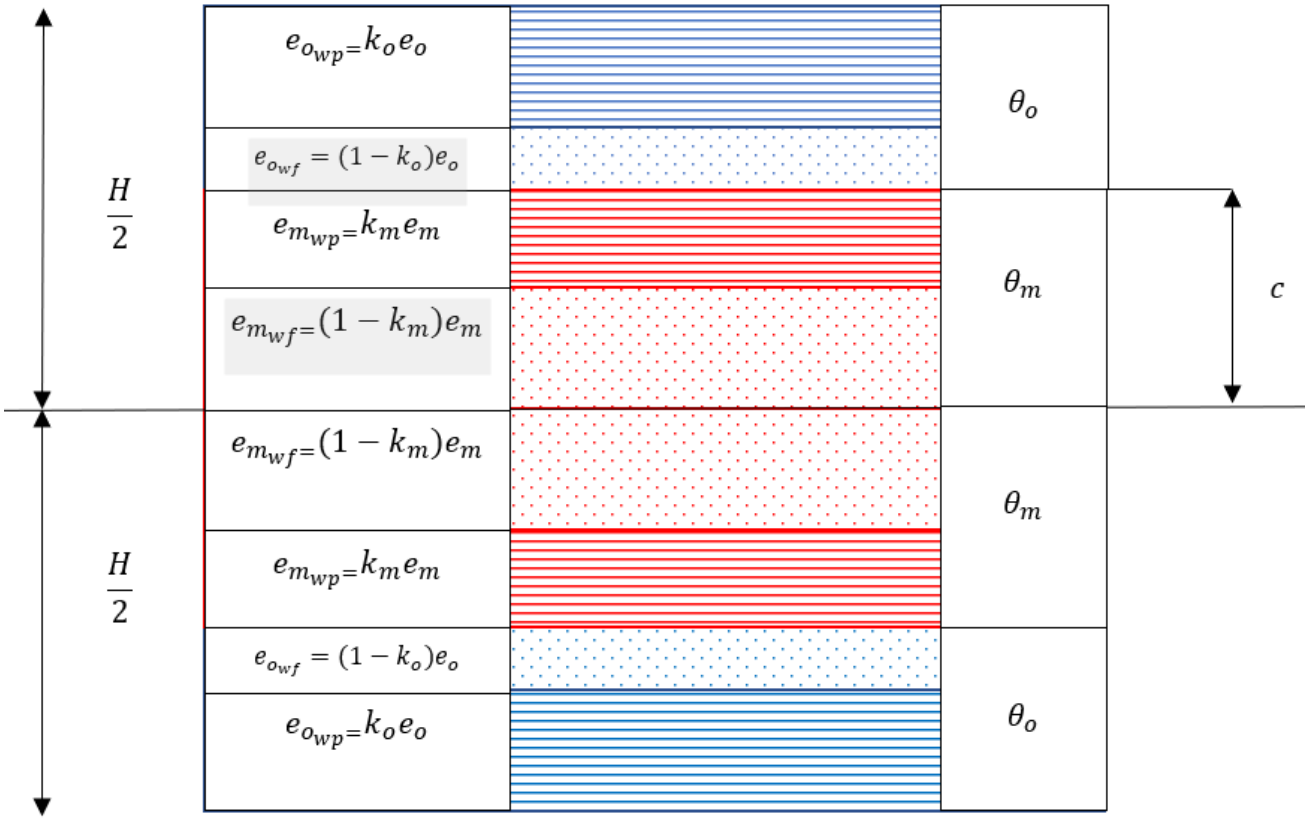

Figure 2. 4-layer, symmetric, woven fibre and graphene platelet reinforced laminate with widths of sublayers and orientation of fibres shown

4.2. Stiffness matrices

Let h_n denote the distance from the midpoint of the laminate to the top of n^{th} layer. The bending stiffness D_{ij} is given by:

$$D_{ij} = \frac{1}{3}\sum_{n=1}^{4} Q_{ijn}\left(h_n^3 - h_{(n-1)}^3\right) \tag{20}$$

Using Figure 2, and the dimensions c and H, D_{ij} is computed as:

$$D_{ij} = \frac{1}{3}\left[2Q_{ijo}\left((-c)^3 - \left(-\frac{H}{2}\right)^3\right) + 2Q_{ijm}(c^3)\right] \tag{21}$$

By introducing the constants d_1 and d_2 such that:

$$d_1 = (-c)^3 - \left(-\frac{H}{2}\right)^3 \;; \quad d_2 = c^3 = e_m^3 \tag{22}$$

D_{ij} can be expressed as

$$D_{ij} = \frac{1}{3}\left(2Q_{ijo}(d_1) + 2Q_{ijm}(d_2)\right) \tag{23}$$

5. Woven fibre/graphene reinforced 3-phase laminate

In the case of 3-phase composites, effective material properties of the graphene and woven fibre reinforced multiscale composite can be obtained by a three-step procedure. First step involves in determining the elastic constants of graphene platelet reinforced matrix for the outer and middle layers, using micromechanical equations, and considering that graphene platelets are uniformly distributed in the matrix. Next, the effective material properties of the 3-phase, graphene reinforced woven fabric will be determined for each of the warp and weft sub-layers of every layer. In the final step, the effective material properties for every outer and middle layer will be determined using equations (4)-(8), providing effective properties between warp-weft sub-layers of woven fabric laminates.

Volume fractions of the graphene platelets in the outer and middle layers are denoted as V_{gpl_o} and V_{gpl_m} and the Young's modulus of the matrix as E_m. Young's moduli of the graphene reinforced matrix in the outer and middle layers, denoted as E_{gm_o} and E_{gm_m} are given by [51]

$$E_{gm_p} = \left(\frac{3}{8}\frac{1+\xi_L\eta_L V_{gpl_p}}{1-\eta_L V_{gpl_p}} + \frac{5}{8}\frac{1+\xi_W\eta_W V_{gpl_p}}{1-\eta_W V_{gpl_p}}\right) \times E_m \tag{24}$$

The geometric factors ξ_L and ξ_W are expressed in terms of the length l_{gpl}, width w_{gpl}, and thickness h_{gpl} of graphene platelets as

$$\xi_L = 2\frac{l_{gpl}}{h_{gpl}}; \quad \xi_W = 2\frac{w_{gpl}}{h_{gpl}} \tag{25}$$

The coefficients η_L and η_W are expressed in terms of the Young's moduli of the graphene, E_{gpl}, and of the matrix, E_m:

$$\eta_L = \frac{\left(\frac{E_{gpl}}{E_m}\right)-1}{\left(\frac{E_{gpl}}{E_m}\right)+\xi_L}; \qquad \eta_W = \frac{\left(\frac{E_{gpl}}{E_m}\right)-1}{\left(\frac{E_{gpl}}{E_m}\right)+\xi_W} \tag{26}$$

Using the mass density of the graphene platelets, ρ_{gpl}, and the mass density of the matrix, ρ_m, the graphene volume fraction can be expressed in terms of its weight fraction W_{gpl} as

$$V_{gpl_p} = \frac{W_{gpl_p}}{W_{gpl_p} + \left(\frac{\rho_{gpl}}{\rho_m}\right)(1-W_{gpl_p})} \tag{27}$$

Denoting the Poisson's ratio of the graphene platelets as ν_{gpl} and the Poisson's ratio of the matrix as ν_m, Poisson's ratio, ν_{gm}, and shear modulus G_{gm} of the graphene reinforced matrix are computed from the expressions

$$\nu_{gm_p} = \nu_{gpl} V_{gpl_p} + \nu_m \left(1 - V_{gpl_p}\right) \tag{28}$$

$$G_{gm_p} = \frac{E_{gm_p}}{2\left(1 + \nu_{gm_p}\right)} \tag{29}$$

Figure 3 shows the 2-phase graphene platelet reinforced laminate before the woven glass fibres are introduced. Material properties, that is, (E_{gm_o}, E_{gm_m}, ν_{gm_o}, ν_{gm_m}, G_{gm_o} and G_{gm_m}) are shown in Figure 3 for each layer. The properties of the graphene reinforced matrix are now used in the micromechanical equations to determine the elastic constants of the 3-phase composite which is further reinforced with woven fibres. Each layer in the woven fibre composite is comprised of two integral unidirectional layers, namely, the warp and weft layers, orientated at 90° to each other.

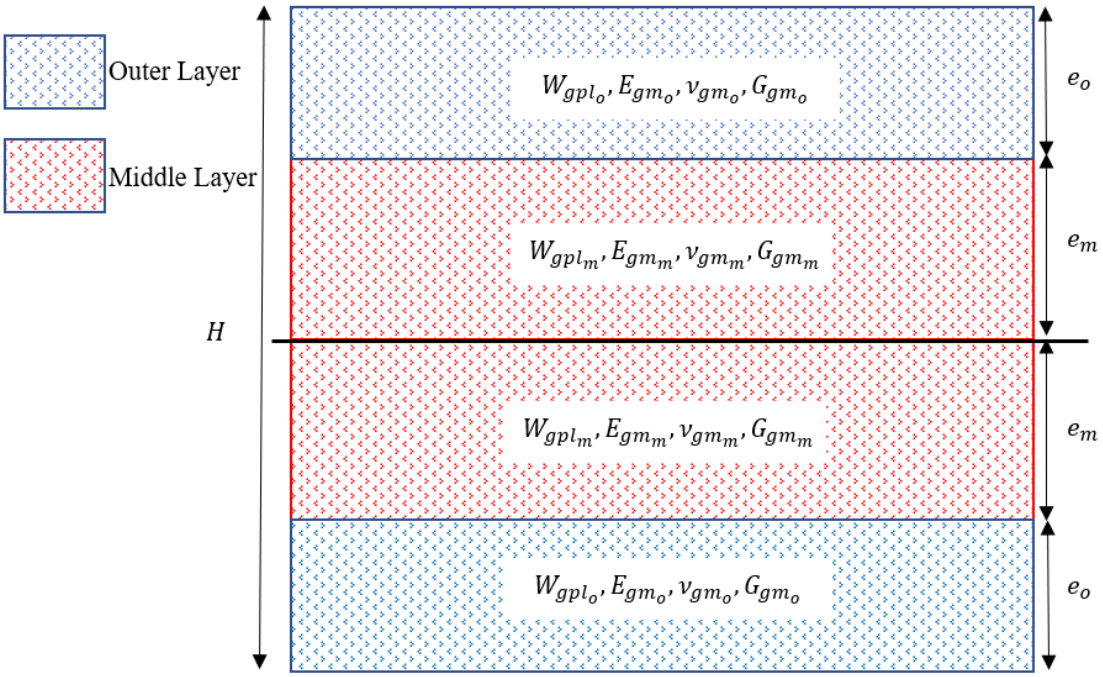

Figure 3. Engineering constants of the 4-ply symmetric laminate with only graphene nanoplatelet reinforcement

In the second step, law of mixtures is used to determine the effective warp layer constants ($E_{11_{wp}}$, $E_{22_{wp}}$, $\nu_{12_{wp}}$ and $G_{12_{wp}}$) and the effective weft layer constants ($E_{11_{wf}}$, $E_{22_{wf}}$, $\nu_{12_{wf}}$ and $G_{12_{wf}}$) for the outer and middle layers of the 3-phase woven fibre/graphene reinforced laminate. Let the subscript $l = wp$ denote the warp layer and $l = wf$ denote the weft layer with E_l denoting the Young's

modulus of the fibres in the warp or weft directions, and Vf_l denoting the volume fraction of the warp and weft fibres. $E_{11_{wp}}$ and $E_{11_{wf}}$ can be calculated using the law of mixtures:

$$E_{11_l} = E_l Vf_l + E_{gm}(1 - Vf_l) \tag{30}$$

Let ν_l denote the longitudinal Poisson's ratio of the warp and weft fibres. The longitudinal Poisson's ratios, $\upsilon_{12_{wp}}$ and $\upsilon_{12_{wf}}$, are similarly calculated as

$$\nu_{12l} = \nu_l Vf_l + \nu_{gm}(1 - Vf_l) \tag{31}$$

Let G_l denote the shear moduli of the warp and weft fibres. Using the cylindrical-cell approach [16], the longitudinal shear moduli, $G_{12_{wp}}$ and $G_{12_{wf}}$, are computed as

$$G_{12_l} = G_{gm}\left(\frac{G_l(1 + Vf_l) + G_{gm}(1 - Vf_l)}{G_l(1 - Vf_l) + G_{gm}(1 + Vf_l)}\right) \tag{32}$$

The lateral compression moduli of the warp and weft layers, $K_{23_{wp}}$ and $K_{23_{wf}}$, are computed using the cylindrical-cell approach [50]:

$$K_{23_l} = \frac{E_{gm}}{2(1 - 2\nu_{gm})(1 + \nu_{gm})} + \frac{Vf_l}{\dfrac{1}{k_l - k_{gm} + \frac{1}{3}(G_l - G_{gm})} + \dfrac{1 - Vf_l}{k_{gm} + \frac{4}{3}G_{gm}}} \tag{33}$$

The bulk moduli of the graphene reinforced matrix, k_{gm}, as well as those of the warp layer, k_{wp}, and the weft layer, k_{wf}, are given by

$$k_{gm} = \frac{E_{gm}}{3(1 - 2\nu_{gm})}; \qquad k_l = \frac{E_l}{3(1 - 2\nu_l)} \tag{34}$$

The transverse shear moduli of the warp and weft layers, $G_{23_{wp}}$ and $G_{23_{wf}}$ are calculated using the 3-phase cylindrical-cell approach

$$G_{23_l} = G_{gm}\left(1 + \frac{Vf_l}{\dfrac{G_{gm}}{G_l - G_{gm}} + \dfrac{k_{gm} + \frac{7}{3}G_{gm}}{2k_{gm} + \frac{8}{3}G_{gm}}(1 - Vf_l)}\right) \tag{35}$$

Transverse Young's moduli of the warp and weft layers, $E_{22_{wp}}$ and $E_{22_{wf}}$, are determined from

$$E_{22_l} = \frac{2}{\frac{1}{2K_{23_l}} + \frac{1}{2G_{23_l}} + \frac{2\nu_{12_l}^2}{E_{11_l}}} \tag{36}$$

In the third step, the effective material properties for each layer of the 3-phase woven fabric laminate will be determined. The equations (4)-(8) will be used in this case, to provide the effective material properties of one warp and one weft sub-layer, for every layer of the laminate. Due to the laminate having symmetrical layers, the two outer layers and the two middle layers have identical properties. Let $p = o$ and m denote the outer and middle layers, respectively. The in-plane longitudinal Young's modulus, E_{11_p}, transverse Young's modulus, E_{22_p}, Poisson's ratio, ν_{12_p} and shear modulus, G_{12_p}, denoting the overall effective material constants of the 3-phase laminate, are given by [50]:

$$E_{11_p} = \left(1 - \alpha_p\right)\left(k_p \alpha_{wp_p} E_{11_{wp_p}} + \left(1 - k_p\right)\alpha_{wf_p} E_{22_{wf_p}}\right) \tag{37}$$

$$E_{22_p} = \left(1 - \alpha_p\right)\left(k_p \alpha_{wp_p} E_{22_{wp_p}} + \left(1 - k_p\right)\alpha_{wf_p} E_{11_{wf_p}}\right) \tag{38}$$

$$\nu_{12_p} = \frac{k_p \alpha_{wp_p} \nu_{12_{wp_p}} E_{22_{wp_p}} + \left(1 - k_p\right)\alpha_{wf_p} \nu_{12_{wf_p}} E_{22_{wf_p}}}{k_p \alpha_{wp_p} E_{22_{wp_p}} + \left(1 - k_p\right)\alpha_{wf_p} E_{11_{wf_p}}} \tag{39}$$

$$G_{12_p} = k_p G_{12_{wp_p}} + \left(1 - k_p\right) G_{12_{wf_p}} \tag{40}$$

Equations (37)-(40) are the elastic constants for the graphene and woven fabric reinforced matrix and are similar to Eqs. (4)-(7) which are the elastic constants of woven fabric only reinforced matrix. The parameters α_{wp_p} and α_{wf_p} are calculated using the Young's moduli and Poisson's ratio of the warp and weft layers and are given by:

$$\alpha_{wp_p} = \frac{1}{1 - \left(\frac{E_{22_{wp_p}}}{E_{11_{wp_p}}}\right)\nu_{12_{wp_p}}^2}; \quad \alpha_{wf} = \frac{1}{1 - \left(\frac{E_{22_{wf_p}}}{E_{11_{wf_p}}}\right)\nu_{12_{wf_p}}^2} \tag{41}$$

The parameter α_p is given by:

$$\alpha_p = \frac{\left[k_p \alpha_{wp_p} \nu_{12_{wp_p}} E_{22_{wp_p}} + \left(1 - k_p\right)\alpha_{wf} \nu_{12_{wf_p}} E_{22_{wf_p}}\right]^2}{k_p \alpha_{wp} E_{11_{wp_p}} + \left(1 - k_p\right)\alpha_{wf} E_{22_{wf_p}} + k_p \alpha_{wp} E_{22_{wp_p}} + \left(1 - k_p\right)\alpha_{wf} E_{11_{wf_p}}} \tag{42}$$

Figure 4 shows the woven glass fibre and graphene platelet reinforced 4-layer laminate with the corresponding characteristics of each layer (E_{11_o}, E_{22_o}, ν_{12_o}, G_{12_o}, E_{11_m}, E_{22_m}, ν_{12_m}, G_{12_m}).

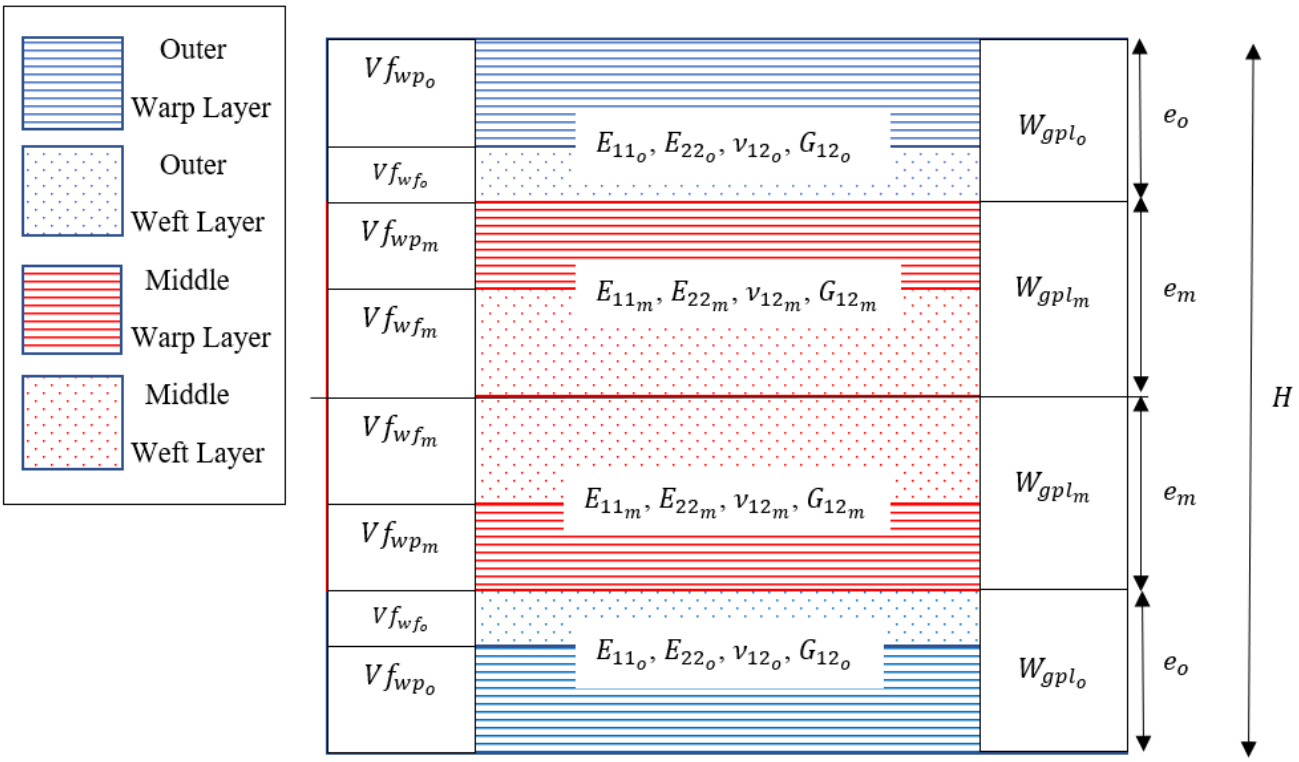

Figure 4. Engineering constants of the 4-ply, symmetric laminate with woven glass fibres and graphene nanoplatelets

6. Verification of the proposed scheme

To verify the adopted formulation, comparisons are conducted between the critical buckling load derived in this article and the ones obtained in [52] and from finite element analysis. In the first comparison, the non-dimensional critical buckling load is $N_0 = b^2 N_{cr}/(\pi^2 D_{22})$ for simply supported, 4-layer laminates with stacking sequence $[0/90]_s$ [52], where N_{cr} is the critical buckling load, b is one of the plate dimensions and D_{22} is a bending stiffness term provided by equation (23). The aspect ratio $R = a/b$ is taken equal to 0.5, 1 and 1.5, and the buckling load ratio $\alpha_b = N_y/N_x$ is 0 (uniaxial compression) and 1 (biaxial compression). Material properties E_1/E_2 varied according to Table 1, $G_{12} = G_{13} = 0.5E_2$, $G_{23} = 0.2E_2$, $\nu_{12} = 0.25$ [52]. All layers are of equal thickness. As given in Table 1, identical buckling loads are obtained between the proposed scheme and [52], indicating that the analytical solution adopted in the article is correctly implemented.

Table 1. Non-dimensional buckling load obtained in the present study and in [52] for simply supported plates

Buckling load ratio $\alpha_b = N_y/N_x$	Aspect ratio $R = a/b$	E_1/E_2				
		5	10	20	25	40
0	0.5	13.900	18.126	21.878	22.874	24.590
	1.0	5.650	6.347	6.961	7.124	7.404
	1.5	5.233	5.277	5.310	5.318	5.332
1	0.5	11.120	12.694	13.922	14.248	14.766
	1.0	2.825	3.174	3.481	3.562	3.702
	1.5	1.610	1.624	1.634	1.636	1.641

To verify the results obtained in the present investigation for 3-phase graphene/fibre reinforced woven fabric laminates, the critical buckling load is compared with the one obtained from finite element analysis. A simply supported, 4-layer laminate is developed in ANSYS commercial finite element software, using 4-node, 3-D shell elements with six degrees of freedom at each node. The material properties for graphene nanoplatelets, glass fibres and the polymer matrix and the non-dimensional buckling load which are used in the subsequent sections of this article, as given in Table 3 and equation (43), respectively, are adopted in the finite element model.

The volume fraction for the warp and weft fibres is taken equal to 0.275 for all layers. The balancing coefficient k denoting the ratio of threads in the warp direction to threads in the weft direction is equal to 0.5, indicating that equal volumes of fibres in the warp and weft directions are considered. The weight fraction of graphene W_{gpl} is 0.01 (1%) for every layer, the laminate thickness ratio τ is taken equal to 0.5 and the laminate aspect ratio a/b is 1 (square plate). Both biaxial and uniaxial compressions are considered, with $\alpha_b = 1$ and $\alpha_b = 0$, respectively.

According to the results shown in Table 2, a similar non-dimensional critical buckling load is obtained from both approaches. It is also shown that as mesh density increases, results of the finite element analysis converge further to the buckling load obtained by the present method.

Table 2. Non-dimensional critical buckling load derived from this article and from finite element analysis using ANSYS commercial software

Finite element analysis	Non-dimensional buckling load	
	Biaxial compression	Uniaxial compression
Mesh size 10x10	39.88	80.40
Mesh size 12x12	39.71	79.41
Mesh size 15x15	39.57	79.13
Present study	39.33	78.65

7. Numerical results

Critical buckling load of the symmetrical laminate based on the classical laminate theory is given by Eq. (15). The non-dimensional buckling load used in the numerical results section is given by

$$N_0 = \frac{b^2 N_{cr}}{E_o H^3} \tag{43}$$

where $E_o = 1$ GPa. In the following numerical section, results are given for biaxial loading ($N_x = N_y$) and for uniaxial loading.

Table 3 gives the material properties of the epoxy matrix [51], the graphene platelets [53] and the glass fibres used for the analysis of the laminate [54]. The length, width and thickness of the graphene platelets are specified as $l_{gpl} = 2.5 \times 10^{-6}$m, $w_{gpl} = 1.5 \times 10^{-6}$m and $h_{gpl} = 1.5 \times 10^{-9}$m [53].

Table 3. Material properties of 4-ply, symmetric laminate

Material	E_{11}(GPa)	E_{22} (GPa)	G_{12} (GPa)	ν_{12}
Graphene	1010	1010	$E_{11}/(2(1+\nu))$	0.186
Glass fibre	72.4	72.4	$E_{11}/(2(1+\nu))$	0.2
Matrix	3.5	3.5	$E_{11}/(2(1+\nu))$	0.35

Effect of the woven glass fibre volume fraction on the non-dimensional critical buckling load N_0 is investigated for different laminate specifications. The parameters investigated include woven fibre concentrations in the warp and weft directions (k_o), the weight fraction of graphene in the laminate W_{gpl_o} and W_{gpl_m}, the laminate thickness ratio τ, and the laminate aspect ratio a/b .

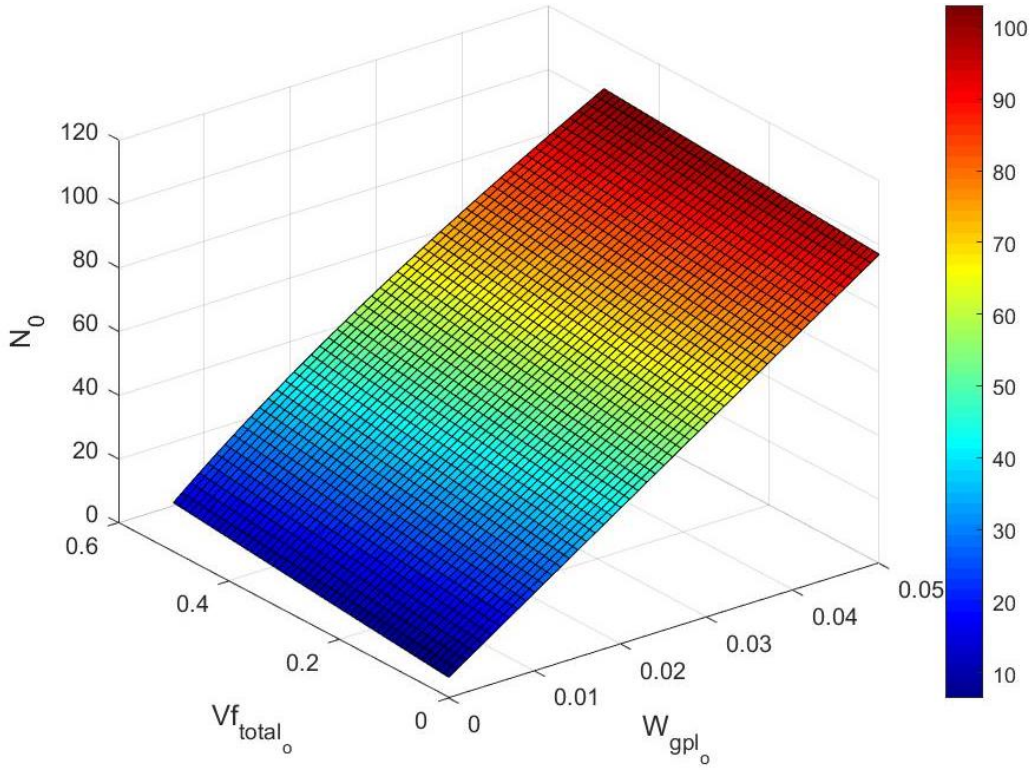

Figure 5. Contour plot of the buckling load vs. Vf_{total_o} for different values of W_{gpl_o} with $\tau = 0.7$; $a/b = 1; \theta_o = \theta_m = 0°; W_{gpl_m} = 0.01; k_o = k_m = 0.5;\ Vf_{total_m} = 0.55; \alpha_b = 1$

The combined effect of increasing both the graphene and fibre contents of the outer layers is investigated in Figure 5 for a square laminate subject to uniform biaxial loads ($N_x = N_y$). It is observed that even a small percentage of graphene is quite effective in increasing the buckling load N_0 as compared to increasing the fibre content of the surface layers. Figure 6 shows the relation between the buckling load and the graphene weight content W_{gpl_o} in the outer layers for different values of the fibre balancing coefficient k_o and for the aspect ratio $a/b = 4$. In order to determine the cross-over point, the graphene content is plotted for the interval $0 \leq W_{gpl_o} \leq 0.1$. It is observed that the cross-over point occurs at $W_{gpl_o} = 0.065$. As the graphene content increases, the higher buckling load occurs at different values of k_o. The highest buckling load is given by $k_o = 0.0$ up to the cross-over point $W_{gpl_o} = 0.065$. After the cross-over point the higher buckling load is given by $k_o = 0.5$ which corresponds to a balanced woven glass fibre distribution.

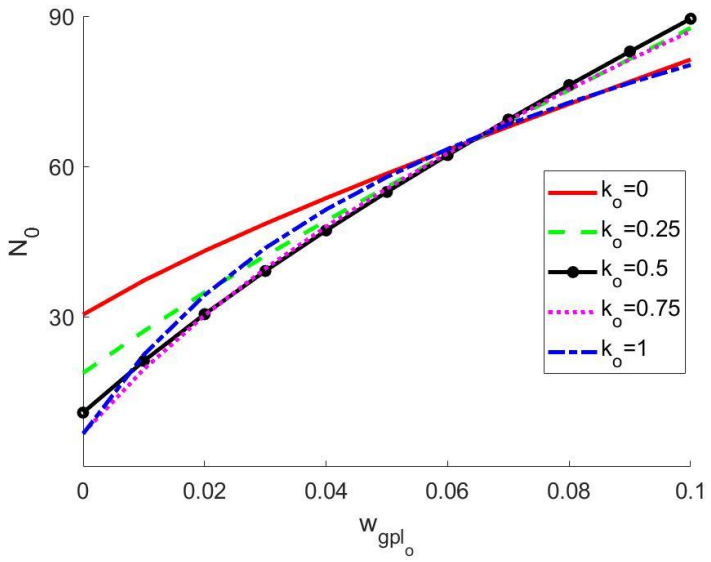

Figure 6. Buckling load vs W_{gpl_o} for different values of k_o with $\tau = 0.7$; $a/b = 4$; $\theta_o = \theta_m = 0°$; $W_{gpl_m} = 0.01$; $Vf_{total_o} = Vf_{total_m} = 0.55$; $k_m = 0.5$; $\alpha_b = 1$

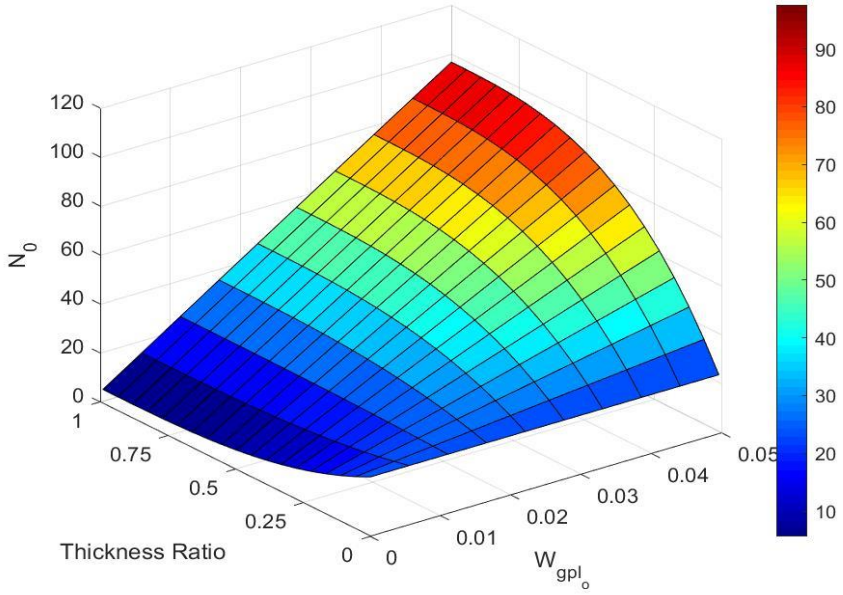

Figure 7. Contour plot of the buckling load against the thickness ratio and W_{gpl_o} for square laminates without woven fabric reinforcement and with $a/b = 1$; $\theta_o = \theta_m = 0°$; $W_{gpl_m} = 0.01$; $k_o = k_m = 0.5$; $Vf_{total_o} = Vf_{total_m} = 0.0$; $\alpha_b = 1$

The contour plot of the buckling load with respect to the thickness ratio and the graphene content of the outer layers W_{gpl_o} are shown for square plates in Figure 7 without any woven fabric reinforcement ($Vf_{total_o} = 0.0$ and $Vf_{total_m} = 0.0$) and in Figure 8 with woven fibre reinforcements of $Vf_{total_o} = 0.55$ and $Vf_{total_m} = 0.55$. It is observed that the effect of graphene on the buckling load increases with increasing thickness ratio as expected. However, for low thickness ratios, the increase in N_o is

minor and the increase in N_o becomes substantial as the thickness of the outer layers increases, i.e., as the thickness ratio increases.

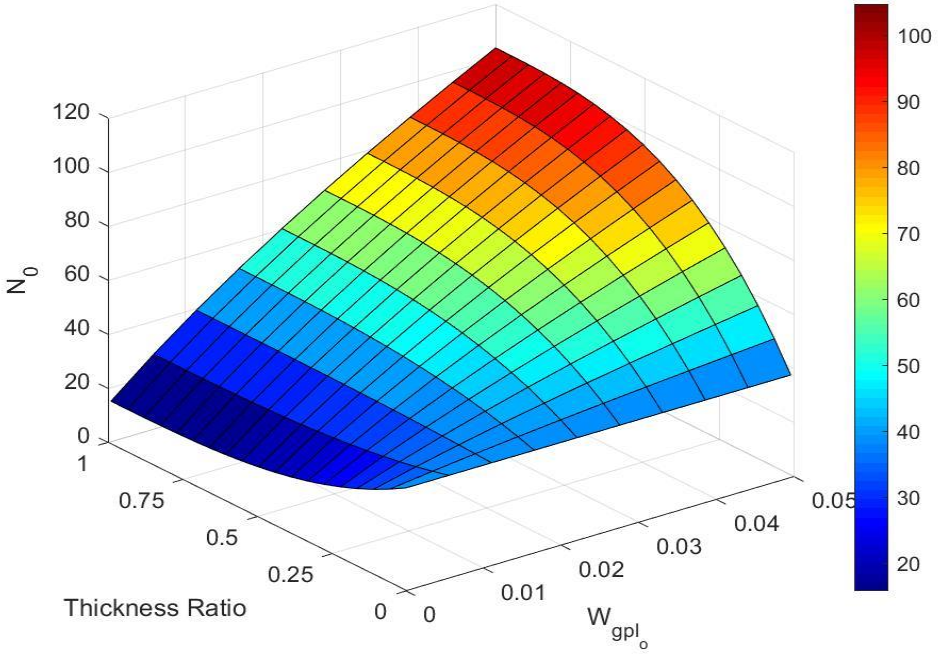

Figure 8. Contour plot of the critical buckling load against the thickness ratio and W_{gpl_o} for square laminates with woven fabric reinforcement, with $a/b = 1$; $\theta_o = \theta_m = 0°$; $W_{gpl_m} = 0.01$; $k_o = k_m = 0.5$; $Vf_{total_o} = Vf_{total_m} = 0.55$; $\alpha_b = 1$

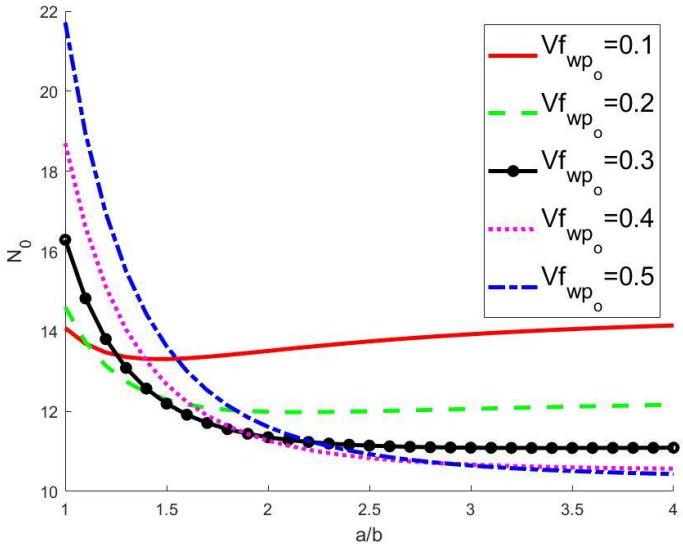

Figure 9. Buckling load vs the aspect ratio a/b for different values of Vf_{wpo} for the laminate with zero graphene content and with $\tau = 0.7$; $\theta_o = \theta_m = 0°$; $k_o = k_m = 0.5$; $Vf_{wf_o} = 0.275$; $W_{gpl_o} = W_{gpl_m} = 0$; $Vf_{total_o} = Vf_{total_m} = 0.55$; $\alpha_b = 1$

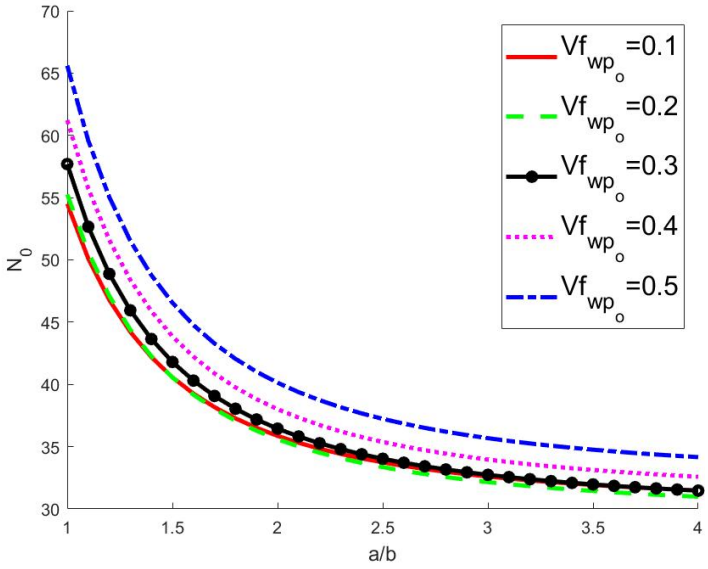

Figure 10. Buckling load vs the aspect ratio a/b for different values of Vf_{wpo} for the laminate with graphene reinforcement and with $\tau = 0.7$; $\theta_o = \theta_m = 0°$; $k_o = k_m = 0.5$; $W_{gpl_o} = 0.02$; $W_{gpl_m} = 0.005$; $Vf_{wf_o} = 0.275$; $Vf_{total_o} = Vf_{total_m} = 0.55$

The influence of graphene reinforcement on the buckling load with respect to aspect ratio and warp fibre reinforcement of the outer layers is investigated in Figure 9 (zero graphene) and in Figure 10 (with graphene) by plotting N_0 vs a/b curves. In the absence of graphene reinforcement (Figure 9), higher buckling loads are given by $Vf_{wpo} = 0.5$ for $a/b \leq 1.6$ and by $V_{fwpo} = 0.1$ for $a/b > 1.6$. When the graphene content is increased to $W_{gpl_o} = 0.02$ (Figure 10), this difference does not appear and $Vf_{wpo} = 0.5$ gives the higher buckling load for all aspect ratios.

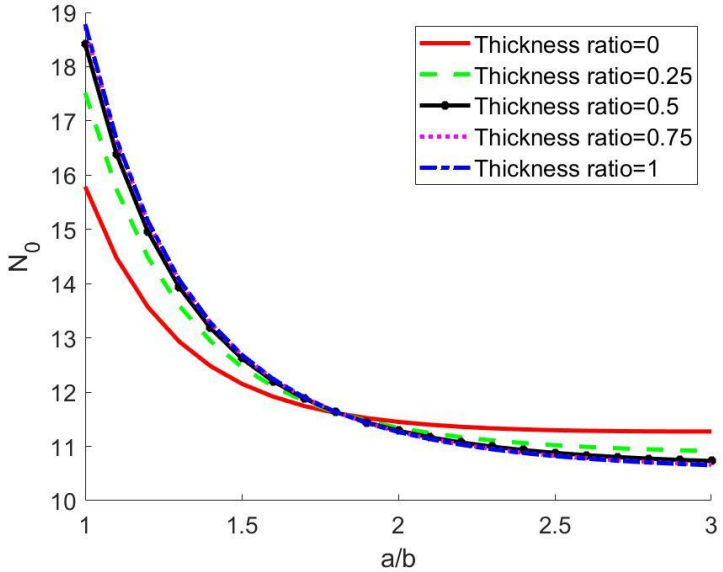

Figure 11. Buckling load vs the aspect ratio a/b for different thickness ratios τ with zero graphene content and with $\theta_o = \theta_m = 0°$; $W_{gpl_o} = W_{gpl_m} = 0$; $Vf_{wp_o} = 0.4$; $Vf_{wf_o} = 0.275$; $k_m = 0.5$; $Vf_{total_o} = Vf_{total_m} = 0.55$; $\alpha_b = 1$

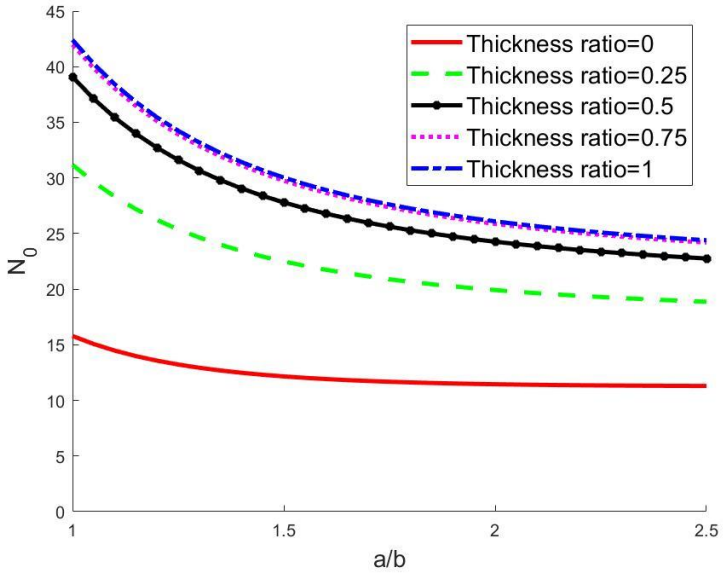

Figure 12. Buckling load vs the aspect ratio a/b for different thickness ratios τ, with the graphene reinforcement and with $\theta_o = \theta_m = 0°$; $W_{gpl_o} = 0.01$; $W_{gpl_m} = 0$; $Vf_{wp_o} = 0.4$; $Vf_{wf_o} = 0.275$; $k_m = 0.5$; $Vf_{total_o} = Vf_{total_m} = 0.55$; $\alpha_b = 1$

Next, the effect of the thickness ratio is studied by plotting the buckling load against the aspect ratio a/b for various thickness ratios in Figure 11 with zero graphene and Figure 12 with graphene reinforcement. In the absence of graphene reinforcement shown in Figure 11, the higher buckling loads correspond to high thickness ratios for $a/b \leq 1.8$. For $a/b > 1.8$, zero thickness ratio gives the higher buckling load which corresponds to a laminate with only the middle layer. However, in the case of a graphene reinforced laminate shown in Figure 12, higher thickness ratio leads to higher buckling loads for the aspect ratios $1 \leq a/b \leq 2.5$.

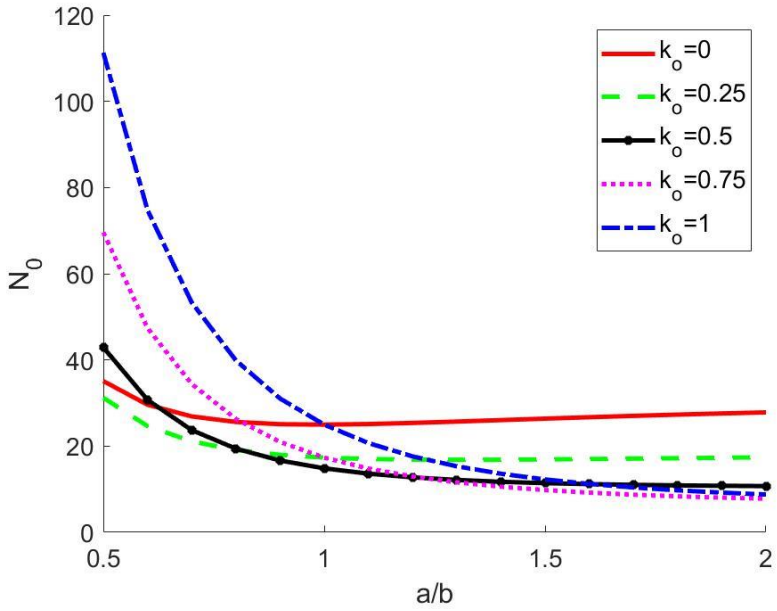

Figure 13. Buckling load vs the aspect ratio a/b for different k_o values for the laminate with zero graphene content and $\tau = 0.7$; $\theta_o = \theta_m = 0°$; $W_{gpl_o} = W_{gpl_m} = 0$; $k_m = 0.5$; $Vf_{total_o} = Vf_{total_m} = 0.55$; $\alpha_b = 1$

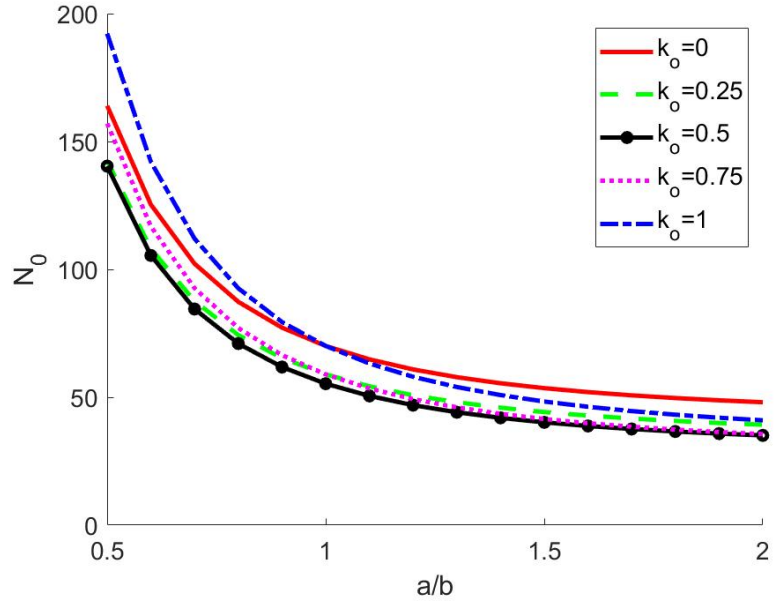

Figure 14. Buckling load vs the aspect ratio a/b for different k_o values for graphene reinforced laminates with $\tau = 0.7$; $\theta_o = \theta_m = 0°$; $W_{gpl_o} = 0.02, W_{gpl_m} = 0.005$; $k_m = 0.5$; $Vf_{total_o} = Vf_{total_m} = 0.55$; $\alpha_b = 1$

The effect of k_o on the buckling load is investigated in Figure 13 (zero graphene content) and Figure 14 (with graphene reinforcement) by plotting the buckling load with respect to the aspect ratio a/b for different values of k_o. In the absence of graphene reinforcement (Figure 13), $k_o = 1$ produces the higher buckling load for $a/b \leq 1$ and $k_o = 0$ for $a/b > 1$. For laminates with graphene

reinforcement shown in Figure 14, $k_o = 1$ gives the higher buckling load also for $a/b \leq 1$ with $k_o = 0$ again giving the higher buckling load for $a/b > 1$ as shown in Figure 14.

Next the effect of the balancing coefficient k_o in the outer layers on the buckling load is investigated by plotting the buckling load against k_o as shown in Figure 15 for different woven fibre contents Vf_{total_o} in the outer layers and for $a/b = 2$. It is observed that the buckling load depends on the fibre contents Vf_{total_o} and the highest buckling loads are given for $k_o = 0.0$ corresponding to the fibres more concentrated in the weft direction. It is also observed that the lowest buckling load is given for a k_o value of $k_o \cong 0.65$, indicating the need to determine the k_o value accordingly for a given aspect ratio to improve the buckling load.

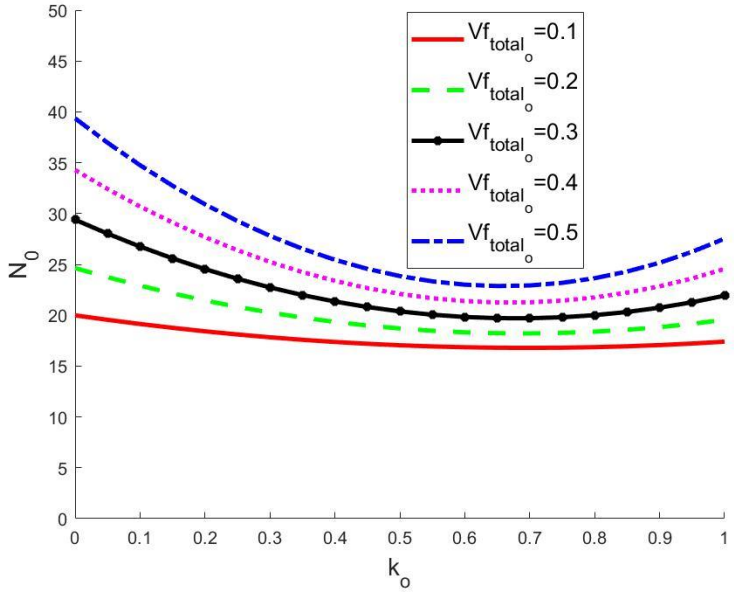

Figure 15. Buckling load vs k_o for different values of Vf_{total_o} with $\tau = 0.7$; $a/b = 2$; $\theta_o = \theta_m = 0°$; $W_{gpl_o} = W_{gpl_m} = 0.01$; $k_m = 0.5$; $Vf_{total_m} = 0.5$; $\alpha_b = 1$

To provide a further insight in the buckling response of the 3-phase woven fabric laminate, the buckling load ratio α_b is taken equal to zero which corresponds to uniaxial compressive loading. In Figure 16, the diagrams of the non-dimensional buckling load versus the volume content of the warp fibres in the outer layers (Vf_{wpo}) are shown for different thickness ratios. It is observed that for all thickness ratios, the (minimum) critical buckling load corresponds to a value of Vf_{wpo} which is approximately equal to 0.125. Similar results as shown in Figure 16 are obtained when the content of the weft fibres is used in the horizontal axis, instead of the content of warp fibres.

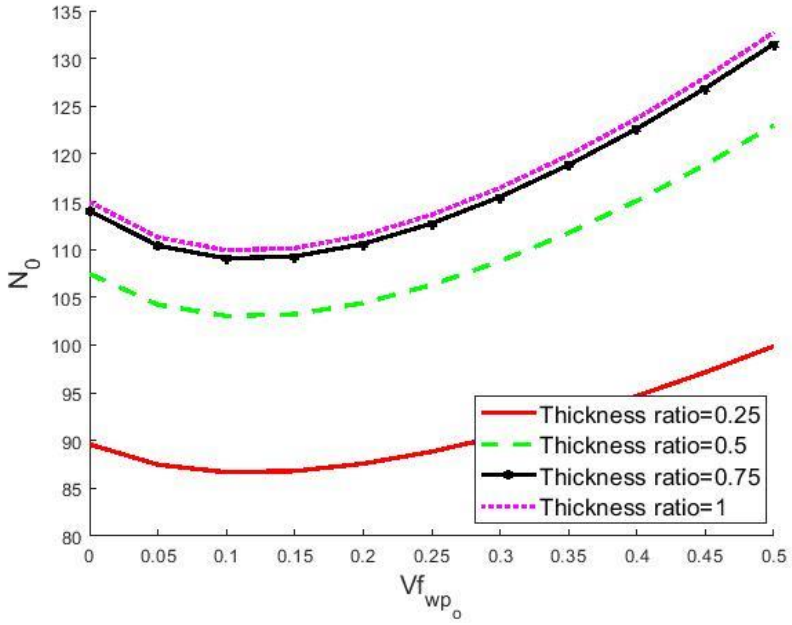

Figure 16. Buckling load vs Vf_{wpo} for different thickness ratios τ and uniaxial compression ($\alpha_b = 0$) with $a/b = 1$; $\theta_o = \theta_m = 0°$; $W_{gpl_o} = 0.02$; $W_{gpl_m} = 0.005$; $k_m = 0.5$; $Vf_{total_m} = 0.55$

In Figure 17 the variation of the critical buckling load versus the graphene weight of the outer layers is shown for different thickness ratio values and for laminates subject to uniaxial compression. Figure 17 indicates that, before the crossover point at $W_{gplo} = 0.01$, laminates with lower thickness ratio and thus, lower outer layer thickness, have higher buckling loads. The reason for this is that the graphene content in the middle layers seems to significantly influence the response, leading to higher buckling loads even for thinner outer layers. For $W_{gplo} > 0.01$ higher buckling loads are obtained for laminates with higher thickness ratios, thus, for higher outer layer thicknesses.

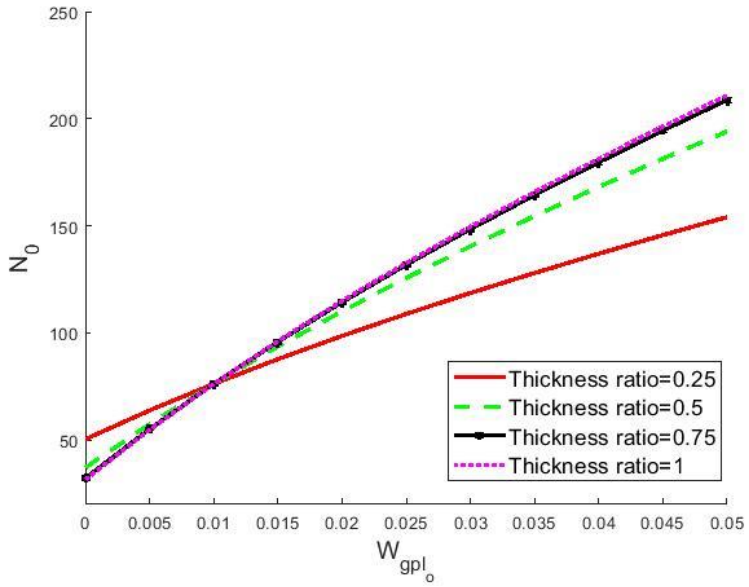

Figure 17. Buckling load vs W_{gplo} for different thickness ratios τ and uniaxial compression ($\alpha_b = 0$) with $a/b = 1$; $\theta_o = \theta_m = 0°$; $W_{gpl_m} = 0.01$; $k_o = k_m = 0.5$; $Vf_{total_o} = Vf_{total_m} = 0.55$

8. Conclusions

Hybrid composite laminates with two reinforcing elements have a number of advantages compared to laminates with a single type of reinforcement as noted in a number of publications [55, 56]. The improvements normally come in the form of higher stiffness and strength and lower weight when a nanoscale reinforcement is combined with a fibre reinforcement [57]. In the present study, hybrid construction is based on reinforcing woven glass fibre laminates with graphene nanoplatelets to improve the buckling load while keeping the weight low. The specific composite studied is a simply supported and symmetrical orthotropic laminate subject to biaxial or uniaxial compressive loads. The results are given to assess the effects of graphene reinforcement and the woven fibre contents as well as the thickness ratios on the buckling load.

Various parameters of the problem affect the buckling load and the maximum buckling load depends on the relative contents of the reinforcements and the thickness ratios for a given aspect ratio. It is observed that, as the graphene content in the surface layers increases, the higher buckling load corresponds to $k_0 = 0.0$ for $W_{gpl_o} \leq 0.065$ and to $k_0 = 0.5$ for $W_{gpl_o} \geq 0.065$ as shown in Figure 6, highlighting the influence of the presence of the warp and weft reinforcements in the outer and inner layers on the buckling load. Thickness ratio between outer and layers is another parameter that affects the buckling load. This issue was investigated in Figure 7 (without woven fibre reinforcement) and in Figure 8 (with woven fibre reinforcement) in order to observe the effect of increasing the thickness ratio and the graphene content on the buckling load. As expected, graphene reinforcement was found to be more effective in increasing the buckling load in the case of hybrid laminates with

the woven fibre included as reinforcement. It was also observed that in the absence of graphene reinforcement, the amount of woven fibre reinforcement determines the aspect ratios at which the highest buckling load occurs (see Figure 9). With the inclusion of graphene in the matrix, the higher buckling loads correspond to highest woven fibre content (see Figure 10). However, in the case of the ratio of the warp and weft layers as indicated by k_o, the highest buckling load is given by $k_o = 1$ for $a/b \leq 1$ and by $k_o = 0$ for $a/b \geq 1$ independent of the graphene content as illustrated in Figures 13 and 14. The use of hybrid constructions in the design of composites can be expected to increase due to the extra flexibility that hybrids offer and also to take advantage of the properties offered by different reinforcements.

The present study can be extended by considering graphene reinforced woven fabric laminates with different boundary conditions and by introducing single or multi-objective optimization schemes, to evaluate optimal values of the design parameters. These tasks are left for future investigations.

References

[1] Ishikawa T, Chou TW. Stiffness and strength behaviour of woven fabric composites. J Mater Sci 1982;vol. 17(11): 3211-3220.

[2] Kim JK, Sham ML. Impact and delamination failure of woven-fabric composites. Comp Sci and Tech 2000;vol. 60(5):745-61.

[3] Stegschuster G, Pingkarawat K, Wendland B, Mouritz A. Experimental determination of the mode I delamination fracture and fatigue properties of thin 3D woven composites. Compos Part A Appl Sci Manuf 2016;vol. 84:308-15.

[4] Long AC. Design and Manufacture of Textile Composites, Woodhead Publishing Ltd, 2005.

[5] Faridul Hasan KM, Horvath PG, Alpar T. Potential fabric-reinforced composites: a comprehensive review. J Mater Sci 2021;vol. 56:14381-415.

[6] Ansar M, Xinwei W, Chouwei Z. Modeling strategies of 3D woven composites: A review. Comp Struct 2011;vol. 93:1947–1963.

[7] Yu Y, Cao Z, Sun Y. Mechanical properties of four types of PVC-coated woven fabrics at high-temperature and after exposure to high-temperature. Structures 2021;vol. 33:830-840.

[8] Kazemianfar B, Nami MR. Can a 3D woven GFRP composite really provide better impact resistance compared to a 2D woven GFRP composite at all of the thicknesses?. Structures 2022;vol. 35:36-45.

[9] Kumar A, Sharma K, Dixit AR. Carbon nanotube- and graphene-reinforced multiphase polymeric composites: Review on their properties and applications. J Materials Science 2020;vol. 55:2682-724.

[10] Mittal G, Dhand V, Rhee KY, Park S-J, Lee WR. A review on carbon nanotubes and graphene as fillers in reinforced polymer nanocomposites. J Industrial and Eng Chemistry 2015;vol. 21:11-25.

[11] Kumar A, Sharma K, Dixit AR. A review on the mechanical properties of polymer composites reinforced by carbon nanotubes and graphene. Carbon Letters 2021;vol. 31:149-65.

[12] Rafee MA, Rafee J, Wang Z, Song H, Yu Z, Koratkar N. Enhanced mechanical properties of nanocomposites at low graphene content. ACS Nano 2009;vol. 3(12):3884-90.

[13] Stankovich S, Dikin DA, Dommett GHB, Kohlhaas KM, Zimney EJ, Stach EA, Piner RD, Nguyen ST, Ruof RS. Graphene-based composite materials, Nature 2006;vol 442:282-86.

[14] Dahiya M, Bansal SA. Graphene-reinforced nanocomposites: synthesis, micromechanics models, analysis and applications – a review. Proc Inst Mech Eng Part C: J Mech Eng Sci 2022;vol. 236(16):9218-40.

[15] Kuilla T, Bhadra S, Yao D, Kim NH, Bose S, Lee JH. Recent advances in graphene based polymer composites, Prog Polym Sci 2010;vol. 35(11):1350-75.

[16] Cho J, Luo JJ, Daniel I. Mechanical characterization of graphite/epoxy nanocomposites by multi-scale analysis, Compos Sci Technol 2007;vol. 67(11):2399-407.

[17] Kim H, Abdala AA, Macosko CW. Graphene/polymer nanocomposites. Macromolecules 2010;vol. 43(16):6515-30.

[18] Young RJ, Kinloch IA, Gong L, Novoselov KS. The mechanics of graphene nanocomposites: a review. Compos Sci Technol 2012;vol. 72(12): 1459-76.

[19] Yasmin A, Daniel IM. Mechanical and thermal properties of graphite platelet/epoxy composites. Polymer 2004;vol. 45(24):8211-19.

[20] Singh V, Joung D, Zhai L, Das S, Hondaker SI, Seal S. Graphene based materials: past, present and future. Progress in Materials Science 2011;vol. 56:1178-271.

[21] Shi G, Araby S, Gibson CT, Meng Q, Zhu S, Ma J. Graphene platelets and their polymer composites: Fabrication, structure, properties, and applications. Adv Funct Mater 2018;vol. 28:1706705.

[22] Civalek Ö, Dastjerdi S, Akgöz B. Buckling and free vibrations of CNT-reinforced cross-ply laminated composite plates. Mech Based Design Struct Mach 2022;vol. 50(6):1914-31.

[23] Chatterjee S, Wang J, Kuo W, Tai N, Salzmann C, Li W, Hollertz R, Nüesch F, Chu B. Mechanical reinforcement and thermal conductivity in expanded graphene nanoplatelets reinforced epoxy composites. Chemical Physics 2012;vol. 531:6-10.

[24] Lee C, Wei X, Kysar JW, Hone J. Measurement of the elastic properties and intrinsic strength of monolayer graphene. Science 2008;vol. 321(5887):385-88.

[25] Mittal G, Dhand V, Rhee KY, Park S-J, Lee WR. A review on carbon nanotubes and graphene as fillers in reinforced polymer nanocomposites. J Indust & Eng Chem 2015;vol. 21:11-25.

[26] King JA, Klimek DR, Miskioglu I, Odegard GM. Mechanical Properties of Graphene Nanoplatelet/Epoxy Composites. J Appl Polymer Sci 2013;vol. 128(6):4217-23.

[27] Shokrieh M, Esmkhani M, Shokrieh Z, Zhao Z. Stiffness prediction of graphene nanoplatelet/epoxy nanocomposites by a combined molecular dynamics–micromechanics method. Comput Mat Sci 2014;vol. 92:444-50.

[28] Anashpaul S, Drosopoulos GA, Adali S. Minimum weight design of CNT/fibre reinforced laminates subject to a frequency constraint. Current Perspectives and New Directions in Mechanics, Modelling and Design of Structural Systems, CRC Press, 2022.

[29] Raju B, Hiremath SR, Mahapatra DR. A review of micromechanics based models for effective elastic properties of reinforced polymer matrix composites. Comp Struct 2018;vol. 204:607-19.

[30] Bacarreza O, Abe D, Aliabadi MH, Ragavan NK. Micromechanical modeling of advanced composites. J Multiscale Model 2012;vol. 4(2):1250005 (20 pages).

[31] Ji X-Y, Cao Y-P, Feng X-Q. Micromechanics prediction of the effective elastic moduli of graphene sheet-reinforced polymer nanocomposites. Model Simulation in Mat Sci Eng 2010;vol. 18:045005 (16pp).

[32] Ishikawa T, Chou T. One-dimensional micromechanical analysis of woven fabric composites. AIAA Journal 1983;vol. 21(12):1714-21.

[33] Tan P, Tong L, Steven GP. Micromechanics models for the elastic constants and failure strengths of plain weave composites. Comp Struct 1999;vol. 47:797-804.

[34] Tanov R, Tabiei A. Computationally efficient micromechanical models for woven fabric composite elastic moduli. J Appl Mech 2001;vol. 68:553-60.

[35] Yang J, Wu H, Kitipornchai S. Buckling and postbuckling of functionally graded multilayer can-reinforced composite beams. Compos Struct 2017;vol. 161:111-18.

[36] Feng C, Kitipornchai S, Yang J. Nonlinear bending of polymer nanocomposite beams reinforced with non-uniformly distributed graphene platelets (GPLs). Compos Part B: Eng 2017;vol.110:132-40.

[37] Thai CH, Ferreira AJM, Tran TD, Phung-Van P. Free vibration, buckling and bending analyses of multilayer functionally graded graphene nanoplatelets reinforced composite plates using the NURBS formulation. Compos Struct 2019;vol. 220:749-59.

[38] Gopalan V, Suthenthiraveerappa V, David JS, Subramanian J, Annamalai AR, and Jen C-P. Experimental and numerical analyses on the buckling characteristics of woven flax/epoxy laminated composite plate under axial compression. Polymers 2021;vol. 13(7):995.

[39] Radebe IS, Drosopoulos GA, Adali S. Buckling of nonuniformly distributed graphene and fibre reinforced multiscale angle-ply laminates. Meccanica 2019;vol. 54(14):2263-79.

[40] Shen H-S, Xiang Y, Lin F, Hui D. Buckling and post-buckling of functionally graded graphene-reinforced composite laminated plates in thermal environments. Compos Part B: Eng 2017;vol. 19:67-78.

[41] Song M, Yang J, Kitipornchai S. Bending and buckling analyses of functionally graded polymer composite plates reinforced with graphene nanoplatelets. Compos Part B: Eng 2018;vol. 134:106-13.

[42] Yang J, Dong J, Kitipornchai S. Unilateral and bilateral buckling of functionally graded corrugated thin plates reinforced with graphene nanoplatelets. Compos Struct 2019;vol. 209:789-801.

[43] Shakouri M, Mohseni A. Buckling analysis of rectangular sandwich plates with functionally graded graphene-reinforced face layers. J Brazilian Society Mech Sci Eng 2020;vol. 42:540.

[44] Song M, Yang J, Kitipornchai S, Zhu W. Buckling and postbuckling of biaxially compressed functionally graded multilayer graphene nanoplatelet-reinforced polymer composite plates. Int J Mech Sci 2017;vol. 131:345-55.

[45] Wu H, Kitipornchai S, Yang J. Thermal buckling and postbuckling of functionally graded graphene nanocomposite plates. Mater Des 2017;vol. 132:430-41.

[46] Song M, Yang J, Kitipornchai S. Bending and buckling analyses of functionally graded polymer composite plates reinforced with graphene nanoplatelets. Compos Part B: Eng 2018;vol. 134:106-13.

[47] Dong YH, He LW, Wang L, Li YH, Yang J. Buckling of spinning functionally graded graphene reinforced porous nanocomposite cylindrical shells: an analytical study. Aerosp Sci Technol 2018;vols. 82-83:466-478.

[48] Wang Y, Feng C, Zhao Z, Yang J. Buckling of graphene platelet reinforced composite cylindrical shell with cutout. Int J Struct Stability Dyn 2018;vol. 18(3):1850040 (17 pages).

[49] Ishikawa T and Chou TW. One-dimensional micromechanical analysis of woven fabric composites. AIAA Journal 1983;vol. 21(12):1714-21.

[50] Berthelot J. Composite Materials Mechanical Behaviour and Structural Analysis, Springer, 1999.

[51] Banerjee S, Sankar BV. Mechanical properties of hybrid composites using finite element method based micromechanics. Comp Part B: Eng 2014;vol. 58:318-27.

[52] Reddy JN (2004) Mechanics of laminated composite plates and shells. Theory and analysis. CRC Press, Boca Raton

[53] Huang Y, Yang Z, Liu A, Fu J. Nonlinear buckling analysis of functionally graded graphene reinforced composite shallow arches with elastic rotational constraints under uniform radial load. Materials 2018;vol. 11(6):910.

[54] Choi S. Micromechanical analysis of composite laminates at cryogenic temperatures. J Comp Mat 2005;vol. 40(12):1077-91.

[55] Sathishkumar TP, Naveen J, Satheeshkumar S. Hybrid fiber reinforced polymer composites: A review. J Reinforced Plastics Comp 2014;vol. 33:454.

[56] Kunwar S, Mer KKS, Joshi A. Mechanical characterization of graphene based hybrid polymer composite with recent applications: A literature review. Int J Sci Eng Research 2015;vol. 6(5):86-96.

[57] Ervina Efzan M.N, and Siti Syazwani N. A review on effect of nanoreinforcement on mechanical properties of polymer nanocomposites. Solid State Phenomena 2018;vol. 280:284-93.